Development of Engineering Assessment Method for Anchorage in Reinforced Concrete

Mattias Blomfors
Industrial PhD Candidate
CBI Swedish Cement & Concrete Research Institute
Box 857
SE-501 15 Borås
Sweden
E-mail: mattias.blomfors@cbi.se

Kamyab Zandi
Associate professor
Chalmers University of Technology

Karin Lundgren
Professor
Chalmers University of Technology

ABSTRACT

There is an increasing need for reliable methods to assess load-carrying capacity and remaining service life of existing infrastructure. Several previous research projects have resulted in a verified, simple 1D model for assessment of anchorage in corroded reinforced concrete structures. Current research aims to extend the 1D model to comprise more practical situations. To verify the 1D model for various cases appearing in practice, such as multiple layers and bundled reinforcement, 3D analyses were carried out. The size of 3D NLFE models required to capture the bond behaviour between corroded reinforcement and concrete is investigated, this to enable efficient analyses. Beam-end models and models of sub-sections with varying sizes and boundary conditions were studied, and the results in terms of bond stress and crack pattern compared. Good agreement was found for several section models; however the choice of boundary conditions largely influence the results and can lead to overestimation of the capacity.

Key words: concrete, corrosion, bond, reinforcement, nonlinear FEA

1. INTRODUCTION

1.1 General

Corrosion of steel reinforcement is the most common cause of deterioration in concrete bridges Bell [1]. Many existing bridges are damaged to varying degrees with corrosion induced cracks or even spalling of concrete cover. The problem with deterioration is also believed to accelerate

in the future due to climate change thus more severe damage can be expected Stewart, Wang & Nguyen [2]. Moreover, the demand on load-carrying capacity of bridges is nevertheless increasing over time. There is therefore a growing need for reliable methods to assess the load-carrying capacity and remaining service-life of existing infrastructure.

Corrosion of reinforcement reduces the cross sectional area of reinforcing bars, and thereby their capacity and ductility. Furthermore, the volume expansion of corrosion products eventually cracks the concrete cover and adversely affects the bond between the reinforcement and concrete; this can result in inadequate anchorage capacity and may cause abrupt failure of the structure. The effect of corrosion on the bond capacity can be modelled using detailed three-dimensional nonlinear finite element (3D NLFE) models, e.g. Coronelli, Zandi & Lundgren [3]. These models are also capable of capturing cracking and spalling of the concrete, but wide practical applications are limited since 3D NLFE analyses require large resources in terms of time and competence.

In order to utilize the knowledge gained from previous research in engineering practice, there is a need for simplified models and tools that are not only accurate enough, but are also time effective for assessment of existing bridges.

1.2 Previous work

A simplified 1D model for the Assessment of anchorage in Corroded Reinforced Concrete structures (1D-ARC) has previously been established. It was originally formulated based on the analytical bond-slip model in Model Code 1990 CEB [4] combined with a parametric study using 3D NLFE analyses by Lundgren *et al*. [5]. The model has later been verified using test results of naturally corroded specimens by Perez *et al*.[6], and validated by 3D NLFE analyses and experiments for high corrosion attacks leading to cover spalling in Zandi [7].

The potential of the 1D-ARC model's practical use has been demonstrated in a pilot study of two bridges by Lundgren, Zandi & Nilsson [8]. It was shown that for these two bridges only, the use of the 1D-ARC model reduced the costs by approx. 27 million SEK as unnecessary strengthening could be avoided. This exemplifies that use of this simplified model can result in enormous cost savings for society.

1.3 Approach

The previously mentioned case study [8] demonstrated great capabilities of the 1D-ARC model; however, it also revealed question marks for the model to be applied in practice. These question marks include applicability of the model on more realistic scenarios commonly seen in bridges, compared to the ones often used in laboratory test set-ups. For that reason it is aimed to validate or further develop the model for the influence of (i) multilayer reinforcement configuration, (ii) spacing between main bars and stirrups, as well as (iii) bundled and spliced bars.

A parametric study of several cases is to be conducted; therefore it is important to make valid simplifications of the computational model to save modelling and computation time. The focus in this paper is put on choosing the level of detail of the 3D NLFE model needed to capture the bond behaviour in an anchorage region of a beam. In particular, the choice of boundary conditions for the simplified model is investigated.

2. STUDIED BEAM GEOMETRY

In order for the assessment tool to be used in practice; it must be applicable to RC beam and slab types commonly seen in bridges. These include several parameters that can vary between structural members, e.g. reinforcement bar diameter, spacing between the reinforcement bars and concrete cover. Furthermore, the reinforcement bars can also be bundled, spliced, and placed in a multilayer configuration. Since corrosion attacks on structures in practice primarily depend on the environmental conditions (location, presence of chlorides etc.), and are not directly associated with the reinforcement layout, the number of situations to be considered in the extension of the 1D-ARC model is large.

The main objective of this paper is to investigate the level of detail required to capture the confining effects from surrounding concrete and stirrups on the bond capacity. Therefore, previously conducted physical tests and detailed 3D NLFE analyses by Zandi, Lundgren & Coronelli [9] of a beam-end were compared to the results obtained from a smaller model of the same geometry.

A beam-end specimen is often used in experimental tests to represent the anchorage region of a beam. It has the shape of an end region of a beam after inclined shear cracking, see Figure 1. A possible source of error for beam-end specimens in general is that the support pressure may increase the confinement around the anchored reinforcement bars and increase the bond capacity. In the test and analyses treated here, the main bars were put in ducts over the supports, i.e. not in contact with the concrete, this to minimize the influence of support pressure and increase the likelihood of anchorage failure.

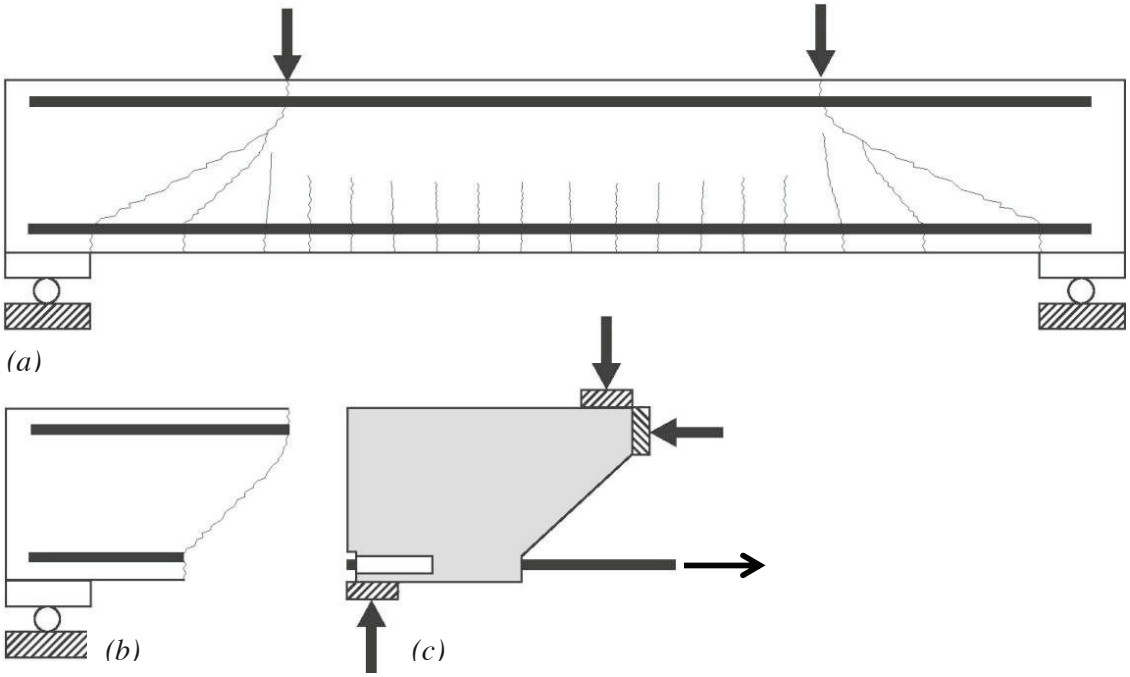

Figure 1: (a) Beam, (b) beam-end specimen and (c) test set-up, adopted from [9].

The studied beam geometry has a square cross-section with 400 mm width and a main bar diameter of 20 mm. One main reinforcing bar is placed in each corner of the cross section with 30 mm concrete cover. An additional bar is placed between the bars in the bottom, giving a total

of three bars to be tested for the anchorage capacity. Load was applied by pulling the bars, and the relative displacement of the reinforcement on both the active and passive side was measured, see Figure 1 c). Two types of specimens which have been subjected to laboratory testing are included in this study: Type A without stirrups and Type B with 8 mm diameter stirrups with 44 mm spacing in the bonded zone. The bonded zone is 210 mm for both beam-end types; see Figure 2.

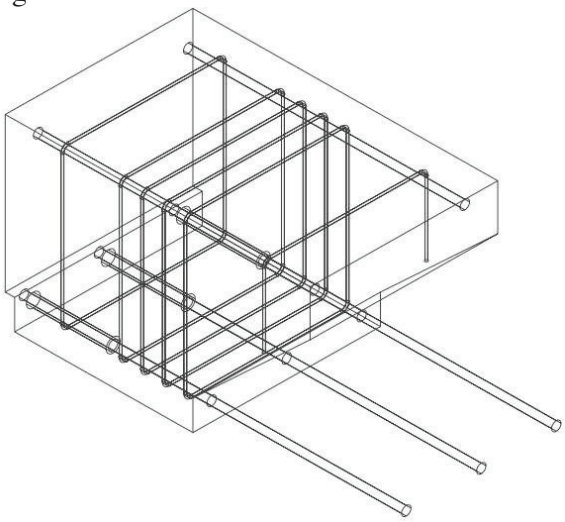

Figure 2: Type B specimen, Type A is similar but without stirrups in the bonded zone

The material parameters for the specimens were tested in [9]. The steel had a yield and ultimate strength of 510 and 610 MPa, respectively, and a Young's modulus of 200 GPa (reinforcement were in elastic range in tests and analyses). The concrete properties, presented in Table 1, vary between the reference and the corroded specimens. This is due to the 3% sodium chloride content in the corroded specimens.

Table 1: Material properties of concrete ($f_{cc,cyl}$ is the average cylinder 28-day strength, f_{ctm} is the mean tensile strength, G_F is fracture energy based on MC 1990, E_c is elastic modulus based on EC 2)

Specimen	$f_{cc,cyl}$ [MPa]	f_{ctm} [MPa]	G_F [N/m]	E_c [GPa]
Reference	27.7	2.2	61.2	28.7
Corroded	29.7	2.3	64.3	29.4

In the FE analyses, a corrosion level of 1.4% weight loss was applied to all bottom bars for the Type A specimen, while for Type B 1.7% was applied for the corner bars and 0.7% for the middle bar. It should be noted that the corrosion levels were larger for the physical experiments. The damage was however similar, this is explained in more detail in [9].

3. NUMERICAL MODELLING OF ANCHORAGE

In this section the bond model for the detailed 3D NLFE analyses is briefly explained. Two types of FE models of different complexity are thereafter presented; one consisting of only a section of the beam and another larger model of the beam-end region. Furthermore, several modelling choices for the smaller model are presented and compared.

3.1 Bond model for detailed 3D NLFE analyses

For the detailed analyses using three-dimensional solid elements the bond model is implemented through the use of interface elements between the reinforcement bar and the concrete. The model is capable of describing both the volumetric expansion of a rebar with the associated normal stresses when steel turns into rust, as well as the normal and bond stresses arising when pulling a corroded bar. A detailed presentation of the bond model for detailed 3D NLFE analyses can be found in Lundgren [10-11]. Furthermore the input parameters for the model were chosen as in Jansson *et al*. [12].

3.2 Model set-up for detailed NLFE analyses

Two detailed 3D FE models of different sizes were set up in DIANA 9.6 [13] and will be presented in the following sub-sections. The first is a larger model of a beam-end region, while the second model is smaller and includes only a section of the beam. A symmetry condition around the vertical axis is used in both cases, reducing the model size to half.

For both models four node, three-side isoparametric solid tetrahedron elements, approximatively 10 mm in size, are used for the concrete and main reinforcement bars. The stirrups are included using embedded elements; this corresponds to full interaction between concrete and stirrups.
The entire circumferences of the main bars were corroded; non-uniform corrosion has been investigated in a previous study by Zandi [7] and is excluded in this study.

For concrete, a constitutive model based on nonlinear fracture mechanics using a smeared rotating crack model based on total strain was applied as TNO DIANA [14]. The crack bandwidth, i.e. the distance over which cracks localize, was assumed to be equal to twice the element size. It was later verified by studying the crack localizations in the analyses. The tensile softening of the concrete was modelled according to Hordijk [15] and the compressive behaviour according to Thorenfeldt *et al*. [16]. For the reinforcing steel an isotropic plastic model was used, together with a von Mises yield criterion. The equilibrium iterations were performed using a Quasi-Newton (BFGS) scheme together with a line search algorithm.

Beam-end model
The beam-end model and boundary conditions are depicted in Figure 3. The load is applied to the bars one at a time, by imposing a deformation on the nodes belonging to the rebar tip. The black triangles represent point supports. The model is fully described in Zandi, Lundgren & Coronelli [9].

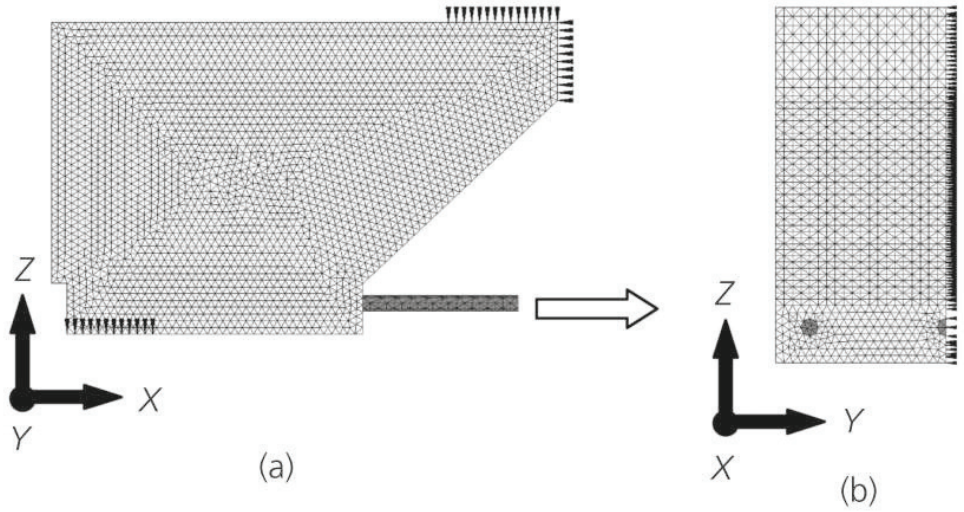

Figure 3: (a) side view, (b) front view of beam-end model

Section model
The section models consist of only a part of the beam-end model. The width and height of the section models are 200 mm and 400 mm respectively, same as the beam-end. Four different models are set up, with varying thickness and/or boundary conditions.

The modelled section geometries are 44, 22 and 10 mm thick, this to investigate the influence of section thickness. The first corresponds to one stirrup spacing and if present, the stirrup is located in the centre of the section. The second geometry corresponds to half of the firstly mention, divided at the centreline. Thus half a stirrup is placed at the back of the section. The third section geometry is 10 mm thick, and the stirrup is placed in the centre with a stirrup area per meter of beam chosen equivalent to that of the bonded zone of the test specimen.

For all section models symmetry boundary conditions (BCs) are applied along the centreline of the section and the nodes on the back (opposite side from where the bars are pulled) are fixed in the pulling direction.

Different BCs are chosen on the front of the sections in order to study different alternatives. Two FE models have the same 44 mm thick geometry, but have different sets of BCs on the front. As representation of the compression zone in a beam-end, one has the nodes in the top 90 mm fixed in the pulling direction. This model is named EL44. The other model has all the nodes on the front free to move but forced to remain in the same plane, which resembles a Bernoulli-region in a beam. This model is named EL44-P. In the 22 mm thick section model no conditions are prescribed to the nodes on the front, this in order to study the influence of restraining the front nodes. This model is named EL22. The 10 mm thick model has similar BCs on the front as EL44, i.e. the thought compression zone is restrained against movement in the longitudinal direction. Furthermore, displacement is prevented in the vertical direction in the centre of one of the bars.

The section models EL44, EL44-P, EL22 and EL10 are depicted in Figure 4 (a)-(d).

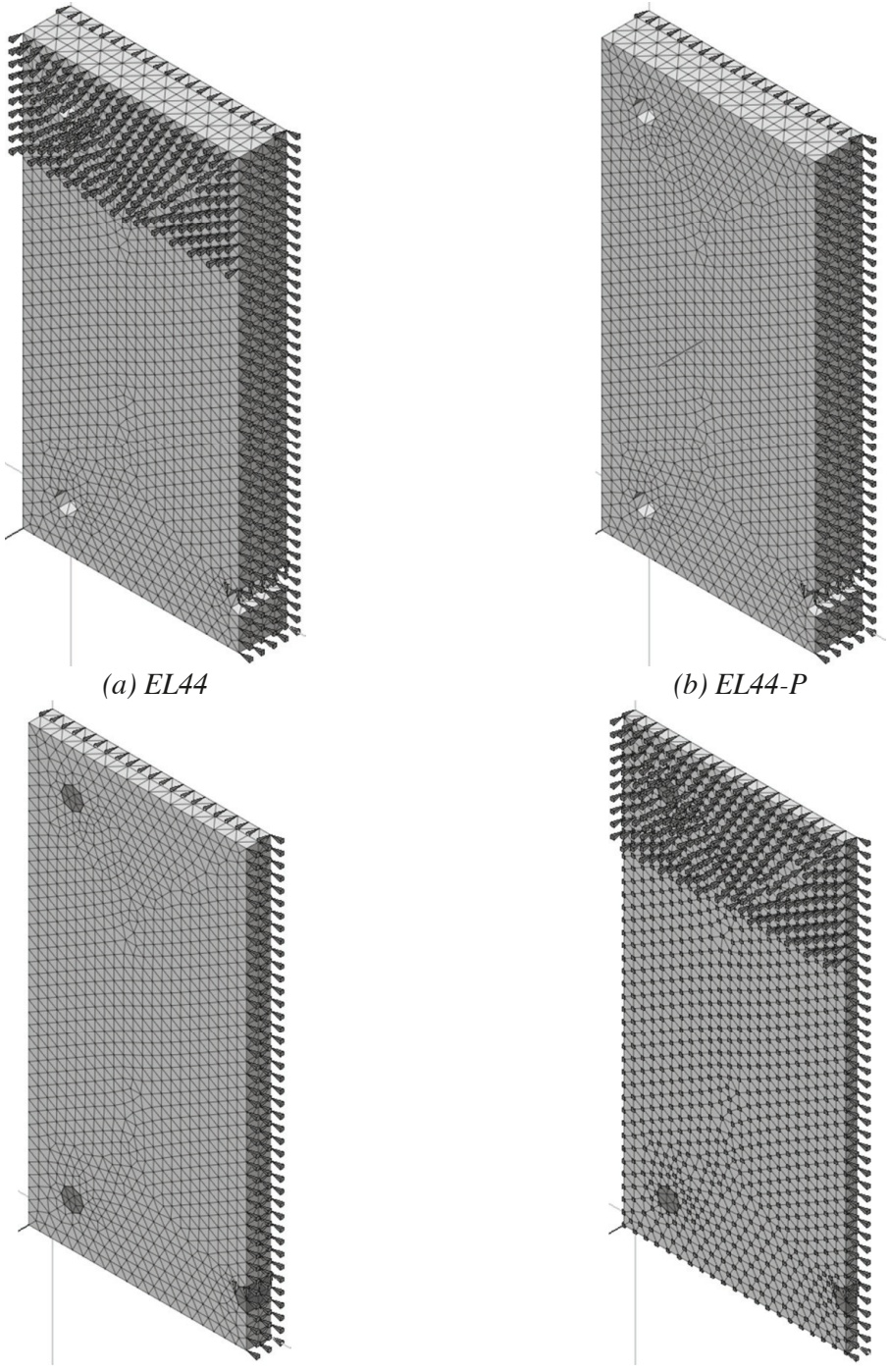

(a) EL44 *(b) EL44-P*

(c) EL22 *(d) EL10*

Figure 4: Depictions of section models; (a) EL44: stirrup in centre, (b) EL44-P: stirrup in centre, front nodes restrained to same plane, (c) EL22: half a stirrup in back, (d) EL10: equivalent stirrup in centre. In (a) and (b) the rebar elements are hidden to better see the element size in z-direction

In the testing procedure the two corner bars were pulled simultaneously, and the middle bar pulled alone. Analogous with the testing procedure and using symmetry conditions, the bars are pulled one by one in the beam-end and section analyses by applying an imposed deformation on

all the end nodes of the pulled bar. The load increment for the section analyses is 0.002 mm/load step.

4. RESULTS

Results from the nonlinear FE analyses of beam sections are presented together with those obtained in previous analyses and tests of beam-end specimens by Zandi, Lundgren & Coronelli [9]. Bond stress curves and crack patterns are presented in the following.

4.1 Bond stress curves

To compare the results from the FE models and tests the average bond stress versus imposed slip of the bar is presented. The average bond stress is for each load step calculated as the reaction force in the pulled nodes divided by the area over which the traction is acting, i.e. the rebar circumference times bonded length.

The results for the Type A and B reference specimens are presented in Figure 5-8 and the corroded cases in Figure 9-11.

Firstly, it is noted that corrosion reduced the maximum average bond stress for all beam-end analyses and tests. For the section analyses the BCs put on the model have a large influence. As a result, the maximum average bond stress could both decrease and increase due to corrosion.

For the Type A reference specimens, see Figure 5 and 6, results in terms of maximum bond stresses from the section models agreed fairly well with test and beam-end values except for EL44-P. This model keeps the front of the section plane, and overestimated the bond capacity for the corner bar. The other three sections showed similar maximum bond capacity, and were in agreement or on the safe side compared to test and beam-end results.

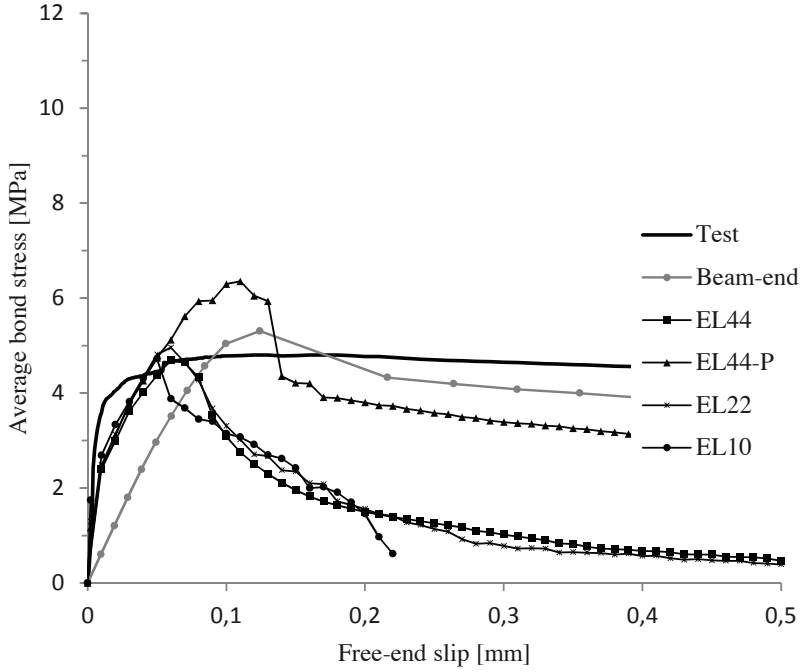

Figure 5: Type A - Reference: corner bar

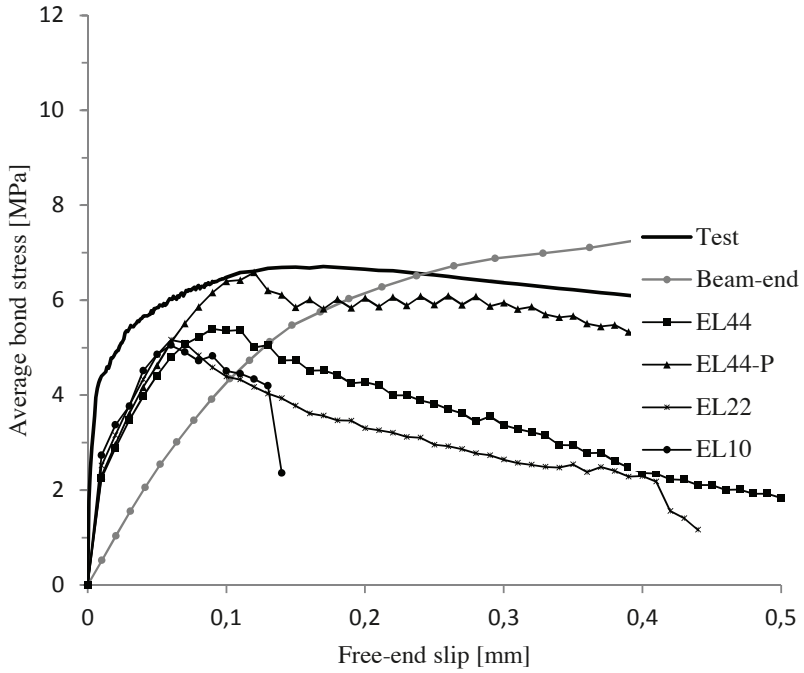

Figure 6: Type A –Reference: middle bar

For the Type B reference specimens, see Figure 7 and 8, the results showed similar patterns as for the Type A specimen. That is, EL10, EL22 and EL44 show similar results, which agree fairly well or are on the safe side compared to tests and beam-end analyses. The EL44-P section

model overestimates the capacity for the corner bar, but agrees well when the middle bar is pulled.

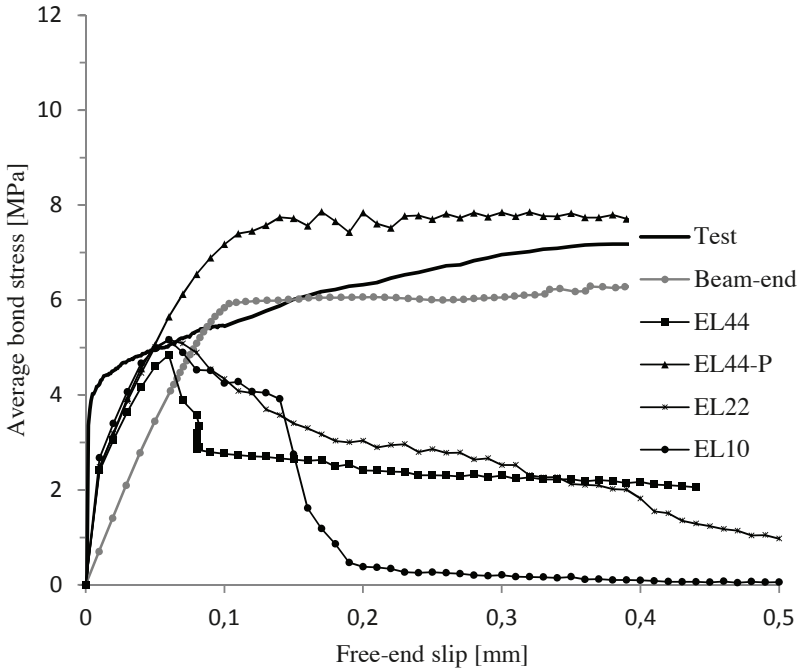

Figure 7: Type B –Reference: corner bar

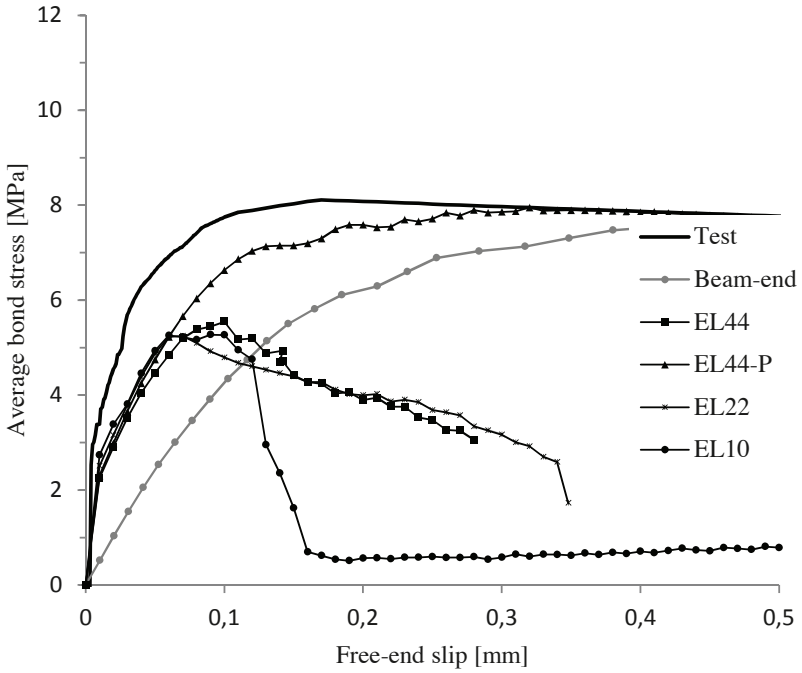

Figure 8: Type B –Reference: middle bar

For the case when 1.4% corrosion was applied to both bars in the Type A specimen (without stirrups), no convergence was obtained for any of the section when pulling the corner bar. This

can be interpreted as if the cover has spalled of the bar, leaving only minor bond capacity. However, when the middle bar was pulled all but EL22 converged. The results are presented in Figure 9.

As previously mentioned, corrosion had an adverse effect on the bond capacity for the test and beam-end model. However, for the section models of the Type B corroded case shows similar or increased capacities. The bond capacity is largely increased for the EL44-P section model, while the other section models show results in line with test and beam-end analyses.

Note that the concrete strength of the reference specimens is slightly lower than for the corroded specimens. However, the beam-end and tests show lower bond capacities if corroded, indicating only small possible influence on the results.

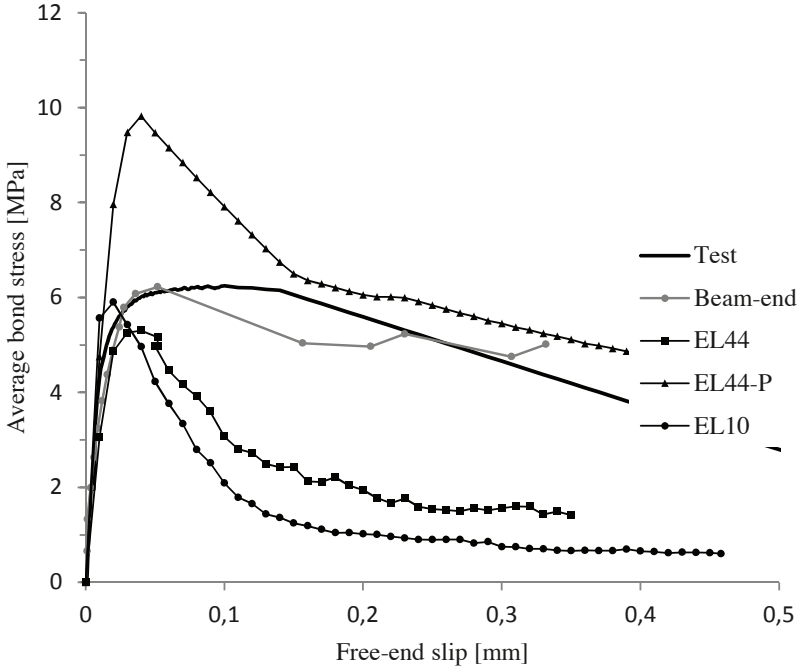

Figure 9: Type A – 1.4% corrosion: middle bar

The results from the corroded Type B specimen are presented in Figure 10 and 11. The beam-end analyses and test values of the bond stress is decreased due to corrosion by around 1-2 MPa. However the EL44-P section model shows an increase in the bond strength of 3 MPa for the middle bar and similar to the reference case for the corner bar. The other three section models produce similar results, which are in agreement with test and beam-end values.

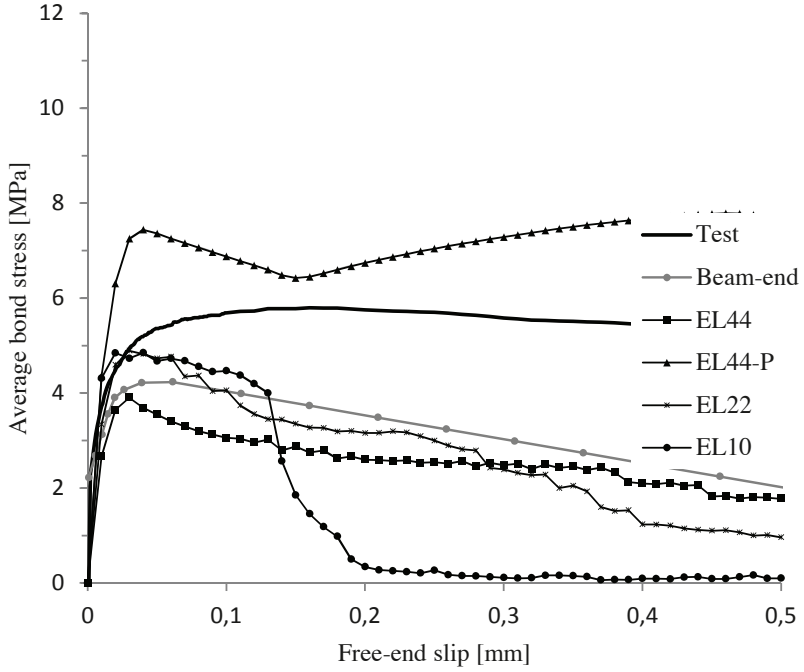

Figure 10: Type B – 1.7% corrosion: corner bar

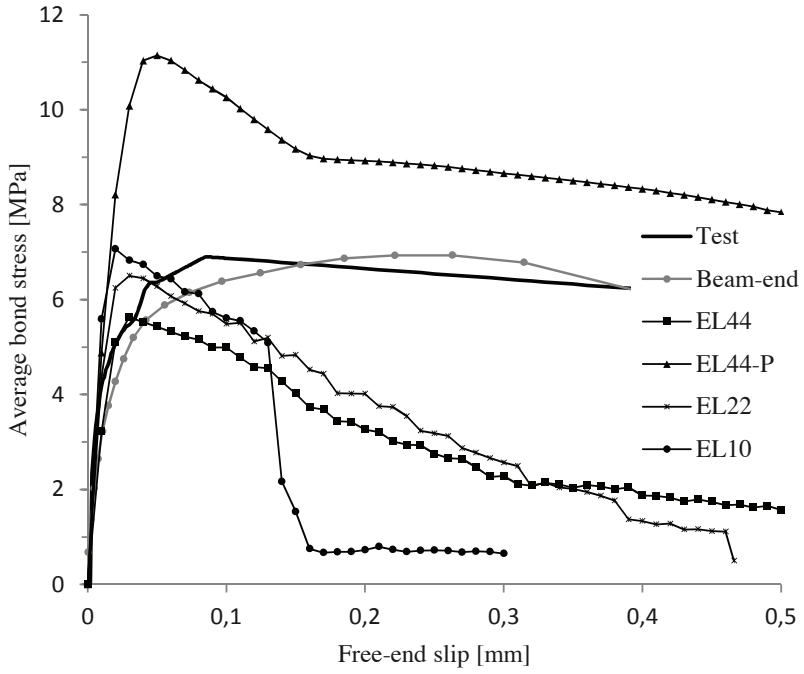

Figure 11: Type B – 0.7% corrosion: middle bar

4.2 Crack patterns

Crack patterns obtained at maximum bond stress from the four different section models are presented in this section. The presented results are of the Type B specimen, i.e. with stirrups, with corrosion applied before pulling the bars individually. Red colour indicates a visible crack (1 ‰ first principal strain), and blue indicates zero strain.

The crack patterns for the two 44 mm thick sections, EL44 and EL44-P, are presented in Figure 12. The crack patterns are similar to those obtained from the beam-end analyses, except for the cracks propagating in the vertical direction. The inclined concrete surface of the beam-end, which thickens the concrete over the height of the specimen, hinders the cracks from propagating upwards. However some vertical cracks, or cracks inclined upwards, are present in the beam-end model. But when present, they are less pronounced in the beam-end model compared to the section model. It should also be noted that the magnitude of the crack widths after the corrosion phase appear to be smaller in the section model compared to the beam-end model for Type B specimens.

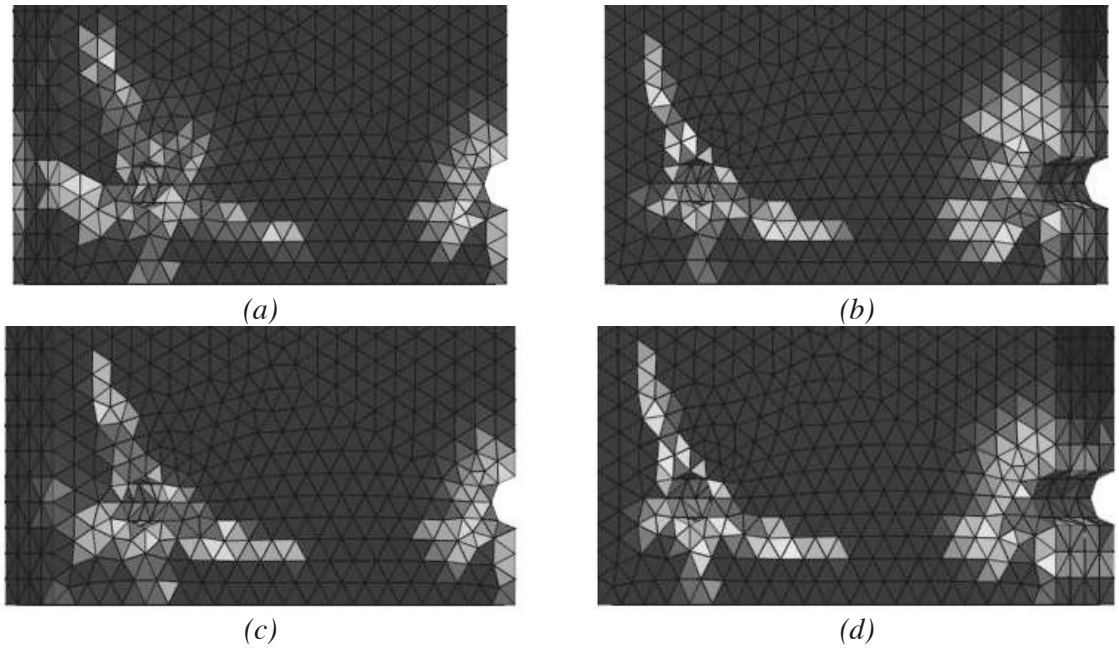

Figure 12: Crack pattern for Type B specimen when subjected to corrosion and bar pull: (a) EL44 - corner bar pulled; (b) EL44 – middle bar pulled; (c) EL44-P - corner bar pulled; EL44-P - middle bar pulled.

The crack patterns for EL22 and EL10 section analyses of the Type B specimen are shown in Figure 13. The 22 mm thick section shows a fairly similar crack pattern compared to the thicker sections, while the 10 mm thick section differs when pulling the corner bar as no crack is propagating downwards. For the 10 mm thick section the horizontal crack to the left is instead more pronounced.

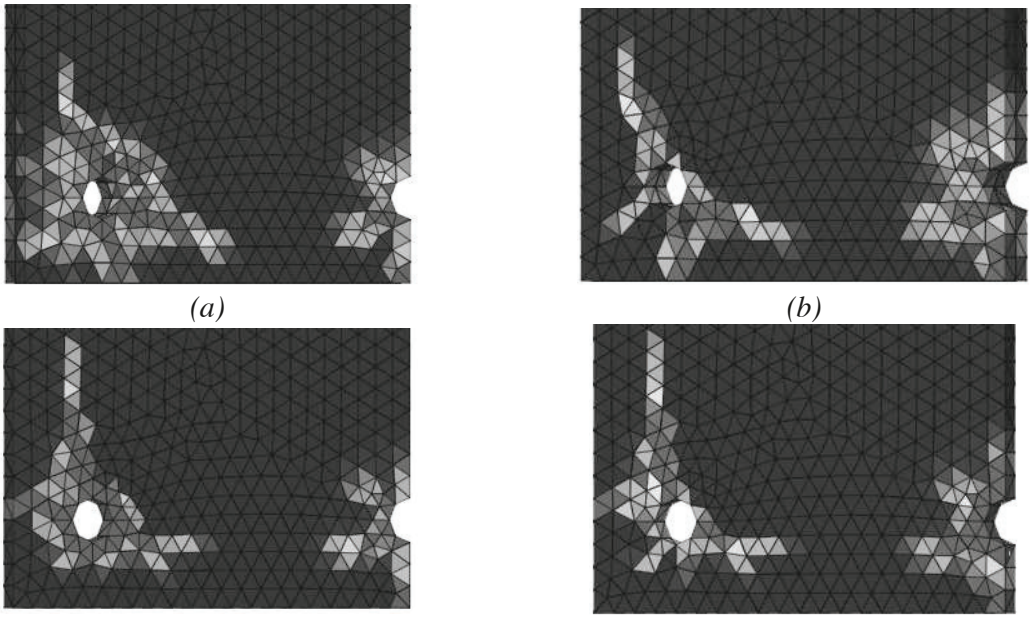

Figure 13: Crack pattern for Type B specimen when subjected to corrosion and bar pull: (a) EL22 - corner bar pulled; (b) EL22 – middle bar pulled; (c) EL10 - corner bar pulled; EL10 - middle bar pulled.

5. DISCUSSION

The results in terms of bond capacity agree reasonably well between the section model, the beam-end model and test for most cases. However, the EL44-P section model where the front was forced to remain plane, showed higher capacity than the beam-end and test values in several cases. The stresses around the pulled bar were studied, and this BC gave rise to compressive stresses around the bar. This is a possible explanation for the difference in bond capacity, since the section models with other BCs showed tensile stresses in the pulling direction around the pulled bar.

The other models EL44, EL22 and EL10 gave fairly similar results, which were corresponding to, or on the safe side, compared to beam-end analyses and tests. However there was a tendency of the thickest model to give slightly lower bond capacity in the case of corrosion than the thinner models. It was checked that the thickness still was small enough to ensure local slip response, so a lower average stress cannot be attributed to varying slip levels along the embedment length. This indicates that the corrosion induced stresses affect the bond of a thicker model more, compared to a thinner model.

The bond stiffness is similar for all section models, and corresponds well to both beam-end and test for the corroded cases. However, for the reference cases all FE analyses give a weaker response than the physical tests. This is due to the calibration of the bond model, which is aimed at capturing the maximum capacity rather than the behaviour at small slip levels. Furthermore, in the representation of the physical test results the free end slip was used. This also contributes to the difference in stiffness compared to the section analyses, where the displacements were obtained from the active end (front of section).

No difference in the bond capacity could be observed between the section models with concrete nodes restrained in the compressions zone (EL44 and EL10) compared to a completely unrestrained concrete front surface (EL22). By studying the stresses it was seen that the restraint at the top 90 mm did not influence the stresses at the bar level, thus the results are reasonable.

An adequate section model simplifies and speeds up the advanced analyses required for the extension of the 1D-ARC model. Furthermore, a section model could also be used to study cases that are particularly hard to model. For instance, a beam-end model with several layers of reinforcement experiences a large anchoring force and is prone to develop an unintended crack at the end of the anchorage length as the tensile capacity of the concrete is exceeded. This study has shown the importance of the boundary conditions when moving from a larger to a smaller model. Furthermore, it will also be investigated if a section model can be used for modelling a region of a beam with spliced reinforcement, a case of large practical interest.

5.1 Conclusions and outlook

The following conclusions regarding bond capacity can be stated based on comparison of results from section analyses, beam-end analyses and experiments:

1) For all considered cases the boundary conditions put on the section model have large influence on the results;
2) Restraining the concrete surface around the bars on the front of the section can cause compressive stresses and lead to excessive capacity;
3) Without corrosion, the capacity were similar or on the safe side for several of the section models;
4) With corrosion, the capacity agreed well for several of the section models, but the section model with concrete restrained around the pulled bars showed too high capacity;
5) The crack patterns were similar in the section and beam-end analyses, as well as in the experiments.

In future work physical, statistical and model uncertainties of the basic variables will be incorporated in the 1D-ARC model. The probabilistic 1D-ARC model will be set up using suitable distribution functions as inputs of the basic variables. Such a model will enable reliability evaluation of different structural elements and also probabilistic service-life prediction. Furthermore, it can also be used to quantify modification factors for the deterministic resistance model, which enables deterministic service-life prediction.

REFERENCES

[1] Bell B. “Sustainable Bridges D1.3 European Railway Bridge Problems”. 2004. Available from www.sustainablebridges.net

[2] Stewart M.G., Wang X., Nguyen, M.N. Climate change impact and risks of concrete infrastructure deterioration. *Eng Struct*. 2011; **33**(4): 1326-1337.

[3] Coronelli D., Zandi Hanjari K., Lundgren K. Severely Corroded RC with Cover Cracking. *J Struct Engineering-ASCE*. 2013; **139**(2): 221-232.

[4] CEB. CEB-FIP model code 1990. *Bulletin d'Information 213/214 CEB*. 1993.

[5] Lundgren K., Kettil P., Zandi Hanjari K., Schlune H., Soto San Roman A. Analytical model for the bond-slip behaviour of corroded ribbed reinforcement. *Struct Infrastruct E*. 2012; **8**(12): 157-169.

[6] Perez I., Tahershamsi M., Marí A.R., *et al*. 1D and 3D analysis of anchorage in naturally corroded specimens. Paper presented at: *Proceedings of the 10th fib International PhD symposium in Civil Engineering; 2014 Jul 21-23; Quebec, Canada*. 2014. p. 547-552.

[7] Zandi K. Corrosion-induced spalling and anchorage capacity. *Struct Infrastruct E*. 2015; **11**(12): 1547-1564.

[8] Lundgren K., Zandi Hanjari K., Nilsson U. A model for the anchorage of corroded reinforcement: validation and application. Paper presented at: *fib Symposium, Concrete - Innovation and Design; 2015 May 18-20; Copenhagen, Denmark*. 2015. p. 1-11.

[9] Zandi Hanjari K., Lundgren K., Coronelli D. Bond capacity of severely corroded bars with corroded stirrups. *Mag Concrete Res*. 2011; **63**(11): 953-968.

[10] Lundgren K. Bond between ribbed bars and concrete. Part 1: Modified model. *Mag Concrete Res*. 2005; **57**(7): 371-382.

[11] Lundgren K. Bond between ribbed bars and concrete. Part 2: The effect of corrosion. *Mag Concrete Res*. 2005; **57**(7): 383-395.

[12] Jansson A., Lofgren I., Lundgren K., Gylltoft K. Bond of reinforcement in self-compacting steel-fibre-reinforced concrete. *Mag Concrete Res*. 2012; **64**(7): 617-630.

[13] TNO DIANA. FEM-software - release 9.6. Delft, The Netherlands. 2015.

[14] TNO DIANA. DIANA finite element analysis user's manual - release 9.6. Delft, The Netherlands. 2015.

[15] Hordijk D.A. Local approach to fatigue of concrete. PhD thesis, Delft University of Technology. Delft, The Netherlands. 1991.

[16] Thorenfeldt E., Tomaszewicz A., Jensen J.J. Mechanical properties of high-strength concrete and applications in design. Paper presented at: *Conference on Utilization of High-strength Concrete*; *Stavanger, Norway*. 1987. p. 149-159.